RSC Advances

ROYAL SOCIETY OF CHEMISTRY

www.rsc.org/advances

RSC Advances

RSCPublishing

PAPER

Probing structural and catalytic characteristics of galactose oxidase confined in nanoscale chemical environments

Cite this: DOI: 10.1039/x0xx00000x

Received 00th XXXXXXXXX 2013,
Accepted 00th XXXXXXXXX 2013

DOI: 10.1039/x0xx00000x

www.rsc.org/

Hideki Ikemoto,[a] Susanne L. Mossin,[a] Jens Ulstrup[a] and Qijin Chi*[a]

Galactose oxidase (GAOX) is a special metalloenzyme in terms of its active site structure and catalytic mechanisms. This work reports a study where the enzyme confined in a nanoscale chemical environment provided by mesoporous silicas (MPS) is probed. Two types of MPS, i.e. SBA-15 and MCF, were synthesized and used to accommodate GAOX. SBA-15-ROD is rod-shaped particles with periodic ordered nanopores (9.5 nm), while MCF has a mesocellular foam-like structure with randomly distributed pores (23 nm) interconnected by smaller windows (8.8 nm). GAOX is non-covalently confined in SBA-15-ROD, while it is covalently immobilized in MCF. Relatively high loading in the range of 50-60 mg/g are achieved. Electron spin resonance (ESR) spectroscopy is used to probe the active site structures of the enzyme. The similar ESR spectra observed for GAOX in the free and immobilized states support that the electronic structure, particularly the copper catalytic centre of confined GAOX is well retained. The catalytic activity of confined enzyme is high, although the catalytic kinetics is slowed down mainly attributed to the diffusion limitation of substrate and product in the nanoscale channels. The apparent Michaelis constant (K_M) of the enzyme is largely unchanged upon immobilization, while the turnover number (k_{cat}) is slightly reduced. The overall catalytic efficiency, represented by the ratio of k_{cat}/K_M, is retained around 70 % and 60% for SBA-15 and MCF immobilization, respectively. The thermal resistance is enhanced up to 60 ^oC, but with no further enhancement above 60 ^oC.

KEYWORDS: *galactose oxidase, mesoporous silica, nanoscale confinement, enzyme biocatalysis, electron spin resonance.*

1. Introduction

Galactose oxidase (GAOX) is a secretory enzyme found mainly in the fungal *Dactylium (D.) dendroides*, *Gibbrewell fujikuroi* and *Fusarium graminearum*.[1] GAOX from *D. dendroides,* which has been mostly studied, is composed of a single polypeptide with a molecular mass of ca. 68 kDa.[1] In view of its active site structure and catalytic mechanisms, this enzyme is widely considered as a very special metalloenzyme. The conspicuous characters of this enzyme include: (a) the enzyme catalyzes the two-electron oxidation of a broad class of primary alcohols to corresponding aldehydes (eq.(1)), coupled by reduction of dioxygen to hydrogen peroxide. However, the enzyme contains only a mononuclear copper ion. The catalytic site thus

has to include an organic cofactor, Y, acting as a second one-electron redox center.[2,3] (b) There are three redox states with distinct activity: fully oxidized (Cu(II)-Y$^{\bullet}$, green), semi-reduced (Cu(II)-Y, blue) and fully reduced (Cu(I)-Y, colorless) forms.[4,5] The fully oxidized and semi-reduced forms participate directly in the catalytic cycle, but the fully reduced form is largely inactive. Moreover, the exact role of the semi-reduced state is still not fully understood, although it is likely to be physiologically relevant.[5] (c) The enzyme has an unusually high isoelectric point (pI) of 12,[6] leading to a significantly positively charged state in almost all buffers commonly used.

$$RCH_2OH + O_2 \rightarrow RCHO + H_2O_2 \qquad (1)$$

The overall catalytic reaction can be split into two half-reactions, i.e., oxidative (eq.(2)) and reductive half-reactions (eq.(3)):

$$RCH_2OH - 2e^- - 2H^+ \rightarrow RCHO \qquad (2)$$

$$O_2 + 2e^- + 2H^+ \rightarrow H_2O_2 \qquad (3)$$

The enzyme has been extensively studied since the late 1950s,[7] but its active site structures and catalytic mechanisms are far from straightforward. The details of these important issues have thus continuously been updated. The latest consensus version of the catalytic mechanisms, as schematically illustrated in Fig. S1 (in the Supplementary Information), has revealed that both the oxidative and reductive half-reactions involve three sub-steps including pure proton transfer (PT), PT coupled to electron transfer (ET), PCET, and pure ET.[8] In addition to fundamental interest in understanding the structures and catalytic mechanisms, GAOX is also of crucial importance in the preliminary diagnosis of galactosemia and galactose intolerance.[9] To construct GAOX based biosensors, immobilization of this enzyme on different supports including macroporous silica has been attempted.[10-12]

Immobilization of enzymes on a support material is essential in many practical applications such as industrial biocatalysis, biosensors, and biofuel cells. Study on the immobilization of enzymes started almost a century ago[13] and has since then been extensively conducted. A variety of methods and supports have been developed and a number of reviews reported. Recently, several review articles by Fernández-Lafuente, Rodrigues and cowokers have systematically addressed multifarious aspects of enzyme immobilization and its applications[14-19]. Hybrid nanostructures offers a new platform for enzyme immobilization[20-21]. Mesoporous silicas (MPS) are one of such attractive materials as described below.

Remarkable progress in the development of new types of mesoporous materials has been achieved in the past two decades, particularly represented by MPS[22-28] and nanoporous colloids[29]. MPS has

demonstrated many attractive physical properties, for example high surface area, excellent stability particularly resistance to high temperature, good mechanical strength, and tunable nanopore sizes (2-50 nm) enabling to match and host a variety of guest molecules. These characteristics have favoured MPS as the immobilization matrix for biomolecules as well. As functional hybrid materials, the bioconjugated MPS could offer combined advantages from silica and biomolecules. MPS offers a host frame with high stability and mechanical strength, while biomolecules provide biological functions such as specific molecular recognition and catalysis. This is of significant interest in biotechnology such as biocatalysis, biosensors, and drug delivery, as the hybrid combination can extend applications of biological molecules beyond their natural mild conditions, i.e., to harsher conditions such as high temperature or the presence of protein denaturing reagents. Since the pioneering work by Diaz and Balkus, in which MCM-41 was used to encapsulate cytochrome *c* (a heme protein),[30] the application of MPS in immobilization of biological macromolecules has been broadly explored, and several reviews have summarized the current status and perspectives.[31-35] More recently (2013), two special themes published in *Chem. Soc. Rev* are devoted to various aspects of mesoporous materials[36-40] and enzyme immobilization[41-43]. In particular, Hartmann and coworkers have systematically summarized the latest progress in enzyme immobilization in MPS and its applications.[44,45] To date about forty enzymes have been attempted to be incorporated as biological guests in different types of MPS hosts, and their stability and catalytic activity in the confined state tested.[34, 44] Focus has been on two types of enzymes, i.e., hydrolytic and redox enzymes, largely motivated by the goal towards efficient production of biofuels and development of highly stable biosensors using enzyme-MPS conjugated hybrid materials.

A recent study of ours has shown that the immobilization of horseradish peroxidase (HRP) in SBA-15 (with 7.6 nm pores) significantly enhanced its thermal and environmental stability.[46] HRP is a relatively small redox enzyme with well-known catalytic mechanism. The present work is focused on GAOX, which is a notably larger enzyme involving complicated catalytic processes. In an early attempt, macroporous silica was used to immobilize GAOX for analytical detection of galactose-containing carbohydrate.[12] Due to incompatible pore sizes (too large, 40-60 nm),[47] however, enzyme leaching was a serious problem and the experimental results were inconclusive. To the best of our knowledge, immobilization of galactose oxidase on mesoporous silica has not been reported before. In the present work, we have synthesized two types of mesoporous silicas and used them as hosts to provide nanoscale chemical environments *with different degree of space confinement for GAOX*. The catalytic activity and kinetics of the enzyme in the free and confined states are compared, and shows that the confined enzyme retains its catalytic efficiency well. The catalytic efficiency depends further on both *the degree of space confinement* and *the immobilization methods*.

2. Materials and methods

Chemicals. GAOX from *Dactylium dendroides* (EC1.1.3.9, lyophilized powder, ≥ 3000 units/g) was purchased from Sigma-Aldrich. Prior to use, GAOX was oxidized by $K_3[Fe(CN)_6]$ (50 mM) and purified on a Econo-Pac 10DG column (Bio-Rad), eluted with sodium acetate buffer (10 mM, pH 4.5) to ensure that the enzyme retains the active oxidized state.

Other reagents including tetraethyl orthosilicate (TEOS) (98% (GC), Aldrich), poly(ethylene glycol)-*block*-poly(propylene glycol)-*block*-poly(ethylene glycol) (Pluronic® P-123, Sigma-Aldrich), D-(+)-Galactose (≥ 99%, Sigma-Aldrich) and cyanuric chloride (99%, Sigma-Aldrich) were used as received. Milli-Q water (18.2 MΩ cm) was used throughout.

Synthesis of mesoporous silica particles. SBA-15-ROD particles were synthesized as follows: 4.0 g Pluronic P123 was added to 144 ml 1.7 M HCl solution and the solution was stirred for 4 hours at 40 °C. 8.0 g TEOS was then added dropwise (the mass ratio of TEOS/P123 = 2) and the mixture was stirred for another 2 hours. The resultant gel was kept at 100°C for 48 hours under static condition.

Mesocellular silica foam (MCF) was prepared according to a previous procedure with modifications.[48] Briefly, about 4 g Pluronic P123 was added to 120 ml 2 M HCl solution and the solution was stirred for 4 hours at 40°C (until Pluronic P123 had completely dissolved). 6 g mesitylene (TMB) and 8.5 g TEOS were then added dropwise under stirring and the polymer–TEOS synthesis mixture was subjected to continuous stirring for 18 h. The resulting gel was kept at 100°C for 24 h under static conditions.

Characterization of mesoporous silica particles. The synthesized mesoporous silicas were characterized systematically by a number of techniques including X-ray diffraction (XRD), TEM, SEM, and nitrogen adsorption-desorption experiments to obtain physical and structural characteristics of the materials. X-ray diffraction (XRD) patterns of the mesoporous silica material were collected on a PANalytical's X'Pert PRO X-ray diffractometer using Cu Kα as radiation. The diffractograms were recorded in the small 2θ range of 0.6° to 5°. SEM images were obtained on an Inspect S or a Helios EBS3 instrument. Silica particles for SEM observation were coated with gold by sputtering to enhance the conductivity. TEM images were obtained using a Tecnai T20 instrument operated at 200 kV. Nitrogen isotherms were measured at 77 K using a Micromeritics ASAP 2020 system. The calcined SBA-15 samples were degassed under vacuum at 200 °C before the nitrogen adsorption measurements.

Functionalization of MCF with amine groups and IR analysis. Amine groups were introduced to the pore walls of MCF by chemical functionalization using a reported procedure[48]. In a typical procedure, 200 mg calcined mesoporous silica was dispersed in 12 ml dried toluene. After addition of 0.137 ml (equivalent to 130.2 mg) 3-aminopropyltrimethoxysilane (APTMS, Sigma-Aldrich), i.e. excess APTMS used in order to achieve saturated amine functionalization, the suspension was refluxed for 3 h. The modified product was recovered by filtration, washed with 40 mL ethanol, and incubated at 80 °C for 1 h.

IR analysis supports chemical functionalization. The FTIR spectrum of MCF before functionalization shows absorption bands in the 3700-3000 cm^{-1} and around 1640 cm^{-1} corresponding to the O-H stretching

and bending modes, respectively, of the silanol groups of the silica particles and/or adsorbed water. After functionalization, the intensity of the 3400 cm^{-1} band decreases and a new peak at 2928 cm^{-1} corresponding to the C-H stretching mode appears. This peak is attributed to the C-H stretching mode of the methylene groups in the $–Si(CH_2)_3NH_2$ (APTMS, 3-aminopropyltrimethoxysilane, moieties) bound on the silica surface, although the absorption of the N-H (primary amine) bending vibration at 1560 cm^{-1} seems too weak to be detected directly.

Preparation of MPS-GAOX conjugates. GAOX was immobilized on mesoporous silicas either by non-covalent trapping or covalent attachment. In the non-covalent trapping, 1 ml of oxidized galactose oxidase (5 μM) in sodium acetate buffer (pH 4.5) was added to a pre-determined amount of silica particles in an eppendorf tube and stirred for 3h. The mixture was centrifuged and the particles washed and re-suspended in sodium acetate buffer (pH 4.5). The adsorbed amount was determined from the absorbance using an extinction coefficient of 1.05 x 10^5 M^{-1} cm^{-1} for the enzyme[8].

The covalent attachment of GAOX to MCF was achieved through surface amino groups of the enzyme covalently linked to the amine-functionalized MCF using cyanuric chloride (CC). Briefly, MCF was first functionalized by the introduction of amine groups as described. The amine containing MCF (50 mg) was then suspended in acetone (3.125 ml), to which cyanuric chloride (25 mg) was added. The mixture was stirred gently for 3 h at room temperature under nitrogen atmosphere and then transferred to a centrifuge tube to remove acetone. The activated silica was transferred to an Eppendorf tube and washed with acetone. 1 ml of enzyme solution was then added and stirred for 2 h at 4ºC. The mixture was centrifuged, and the solid product washed thoroughly with water and stored at 4ºC. The enzyme load was estimated as 46 mg/g silica from UV-vis spectra.

Electron spin resonance spectroscopy. ESR (or EPR) measurements were conducted on a JEOL continuous wave spectrometer JES-FA200 equipped with an X-band Gunn oscillator bridge, a cylindrical mode cavity and a helium cryostat. For all the samples the key experimental parameters used were: modulation frequency 100 kHz, time constant 0.1 s, frequency 8.97 GHz – 9.00 GHz, modulation amplitude 4 G. The simulations were performed using the spin Hamiltonian based program W95epr of Frank Neese (QCMP 136 from the Quantum Chemistry Program Exchange) as reported by Neese and co-workers[49]. The spin Hamiltonian is axial and given by eq(4):

$$H = g_{\|}\,\mu_B\,S_z\,B_z + g_{\perp}\,\mu_B(\,S_x\,B_x + S_y\,B_y) + A_{\|}\,S_z\,I_z + A_{\perp}(\,S_x\,I_x + S_y\,I_y) \qquad (4)$$

where μ_B is the Bohr magneton, B_i , S_i and I_i (i = x,y,z) are the components of the magnetic field, i.e. the spin electron spin operator and the nuclear spin operator along the molecular axes, respectively. $g_{\|} = g_z$ and $g_{\perp} = g_x = g_y$ are the electronic g-values. $A_{\|} = A_{\|} = A_z$ and $A_{\perp} = A_x = A_y$ are the nuclear hyperfine coupling constants to the Cu (63/65) isotopes which both have I = 3/2. The difference in coupling between the

individual isotopes is not resolved. The fittings were performed by the "chi by eye" approach. Line widths were in the range of 20 – 40 Gauss, and the line shapes taken as Lorentzian. A field dependent line width (A strain) was used for the isotropic spectra.

Assays of enzyme activity. Catalytic activity of GAOX was measured using a Commercial Clark-type electrode (YSI 5300A, Biological Oxygen Monitor). The experimental setup is schematically illustrated in Fig. S2 (Supplementary Information). The sample solution was stirred at 480 rpm and the electrode calibrated in air-saturated (0.252 mM O_2)[50]. Milli-Q water. In each measurement, air bubbles were excluded before the start of the measurement. 50 µl of free or immobilized enzyme (stored on ice) was injected into a 3 ml reaction mixture of air-saturated 5-400 mM galactose and 1 mM $K_3[Fe(CN)_6]$ in buffer (pH 7.0) at 25°C through the access slot using a syringe. Since GAOX takes three forms, interconversion between active and inactive forms may take place. To avoid this, hexacyanoferrate (III) was included in the mixture to re-activate inactivated enzyme during the activity assays.

The thermal stability of GAOX was examined by heating the samples including free enzyme solutions and MPS-GAOX conjugated samples at 50-70 °C for 30 min. The solutions were then cooled to room temperature, followed by the assays of catalytic activity. The overall procedure is similar to those used in our previous study for HRP.[46]

3. Results and discussion

D. dendroides GAOX contains a single polypeptide chain consisting of 639 amino acid residues with a molecular mass of 68 kDa.[1] The 3D crystallographic structure reveals that the polypeptide is folded into three domains with the copper catalytic center located in Domain II (Fig. 1a).[3, 51] In the active site region, the Cu ion is coordinated to two tyrosines (Tyr272 and Tyr495), two histidines (H496 and H581) and a solvent ligand (water), Fig. 1b, forming the inner coordination sphere (a Type 2 centre). Importantly, Tyr 272 is covalently bonded to Cys 228 via a thioether bond and its radical form (Tyr$^{\bullet}$272) serves as a catalytic cofactor (i.e., the second redox site). Furthermore, Trp290 stacks over the Cys 228 side chain and plays an essential role in generating Tyr$^{\bullet}$272 radicals for maintaining the enzyme catalytic cycles.[52] Due to its unusually high pI (ca. 12), this enzyme is thus considered to have significantly cationic nature under the experimental conditions used in most studies (Fig. 1c). The 3D dimensions of this enzyme, estimated as 8.4 nm x 6.2 nm x 6.4 nm (Fig. 1d), are large among globular enzymes.[3]

In the following sections, the physical and structural properties of mesoporous silicas are first summarized. This is followed by a discussion of enzyme loading into porous materials. We then present and discuss the EPR spectra. Finally, the catalytic activities under various conditions are compared and discussed.

Physical and structural features of the as-synthesized mesoporous silicas. As noted, two types of mesoporous silicas were used. One is rod-shaped denoted as SBA-15-ROD. The other one, denoted as MCF, was synthesized using TMB as pore expanding agent. The as-synthesized mesoporous materials were characterized systematically by SEM, TEM, XRD, and nitrogen adsorption/desorption. The major physical and structural features

are summarized in Table 1 and Figs. S3-S5 in Electronic Supplementary Information (ESI). SBA-15-ROD contains ordered arrays of cylindrical pores with a diameter of 9.5 nm. TEM images reveal that the nanopores run in one dimension with no interconnection between pores. MCF has a mesocellular foam-like structure with significantly larger pores (23 nm) and tends to be of spherical shape, though its morphology is less well-defined. The main nanopores (also called cells) are interconnected by smaller openings (i.e., windows, 8.8 nm) to form a three-dimensional pore network.

Encapsulation of enzyme into MPS. GAOX (oxidized form) was loaded into SBA-15-ROD and MCF silica particles as described. To check the enzyme stability under stirring conditions, the solution containing only free oxidized GAOX was stirred for 3 h. Oxidized GAOX was stable during immobilization (data not shown). To load enzyme, the mixture of particles and GAOX solution was stirred for 3 hours. When the initial ratio of protein to particles of 125 mg protein per g particles in the solutions was used, similar amounts of GAOX was found to be adsorbed onto both types of particles, i.e. about 62 mg protein per g particles for SBA-15-ROD and 58 mg protein per g particles for MCF (Table 1). When the initial ratio of protein to particles is increased to 250 mg protein/g particles, the GAOX loading in MCF was enhanced to 89 mg protein per g particles but with no further increase of GAOX loading for the SBA-15-ROD. This difference is most likely caused by two key factors: (1) different pore structures in the two types of silicas and (2) The unusually high pI of 12 of GAOX. Since the loading experiments for immobilization of GAOX to silica particles were performed using sodium acetate buffer (pH 4.5), GAOX is in cationic state. Lateral repulsion between protein molecules would be stronger at pH 4.5 at higher initial ratio of protein to particles. The pore entrance sizes for the two types of MPS are similar (9.5 nm for SBA-15-ROD vs. 8.8 nm for MCF), but the pore structure is significantly different (hexagonally ordered cylinder vs. cage-type pores). The cage structure may isolate a given GAOX molecule from the rest of the GAOX molecules, thereby alleviating the strong lateral repulsion between the protein molecules. The loading of this enzyme is modest to high, compared to reported values for other enzymes. For example, HRP loading on SBA-15 is about 24 mg g^{-1} particles[46, 53] and 44 mg g^{-1} on SBA-15 for lipase but is enhanced to 91 mg g^{-1} on PMO[44,45]. The entrance to the cylindrical pores for SBA-15-ROD are further exposed to the GAOX solution at both ends of the rods and the entrances hexagonally packed. In the case of MCF, entrances (windows) are located away from each other and distributed over the surface that is exposed to the GAOX solution. This different arrangement of entrances would also affect protein adsorption to the pores.

It remains a challenge to identify the exact location of immobilized biomolecules in MPS. In the present case the enzyme is most likely located inside the pores, as supported by both nitrogen adsorption experiments and the relatively high loading amount (modest but not low). However, an interesting question is thus raised how other enzyme molecules can go inside the pores to yield the observed loading amount, once a molecule of enzyme become immobilized at the end of the pore. The precise answer to the question has been elusive, although there are a great number of studies on enzyme-MPS systems reported. We here attribute the experimental observations to the two main possible reasons: 1) enzyme loading is a dynamic process, which is assisted by stirring solution; and 2)

the pore diameter most likely increases in the aqueous solution due to partial solubilization of silica, which facilitate enzyme moving and increases the loading amount. Enzyme loading into the pores is a dynamic process until equilibrium is established, and different enzyme strengths of the enzyme molecules to the pore walls would prevail in the loading process. A first enzyme molecule captured at the pore entrance would therefore move along the channel towards the particle interior leaving space for new enzyme molecules to become immobilized. Loading would thus be continued. This random walk, or one-dimensional surface diffusion mode, sometimes colloquially called the "bucket brigade mechanism" would follow views on transport in biological membrane pores, fuel cell pore materials, and other contexts. Stirring solution helps dynamic migration of enzyme molecules along the channels, as evidenced by the fact that simple mixture MPS particles and enzyme in solution without stirring yield considerable low loading amount (about 30-40%).

Nitrogen adsorption experiments can be used to identify the enzyme loading, as nitrogen adsorption is reduced upon immobilization of the enzyme [54, 55]. A comparison of the nitrogen adsorption isotherms of particle samples before and after enzyme immobilization is shown in Fig. S5 (in ESI). The surface area and pore volume of the MPS particles are both decreased significantly after stirring of the MPS particles in the pure buffer solution (i.e. in the absence of enzyme) for 3 hours (Table S1, Supplementary Information). The presence of enzyme in the buffer solution causes a further decrease in both surface area and volume (Table S1), but the volume decrease is not significant. The former is likely due to partial loss of the micropores in the MPS particles by stirring, resulting from solubilisation of the silica with a positive radius of curvature at the micropore entrance and subsequent redeposition of the solubilized silica inside the micropores.[56] Thus, the actual size of the MPS pores in wet condition is larger than that measured in the dry state by nitrogen adsorption. The increase of the pore size is ca. 15%[56]. On the other hand, since the loading of GAOX (ca. 60 mg per g particles, i.e. 6 % by wt) was at a modest level, it is thus not surprising that further decrease in surface area and total volume of the pores upon encapsulation of enzyme is not significant. Based on these observations, Figure 2 illustrates schematically the structures of SBA-15-ROD and MCF and confinement of GAOX in the MPS pores.

Electron spin resonance analysis. No defined technique is currently available for *direct probing of the details* concerning the distribution, organization and 3D-structures of biological macromolecules confined inside the MPS pores. In some recent efforts, fluorescence spectroscopy/microscopy[57] and EPR spectroscopy[58] have, however, emerged among few promising techniques that could offer structural information of biomolecules confined in MPS. EPR was employed in the present study to explore the structures of GAOX confined in nanoscale channels with a focus on the active catalytic site around the copper centre.

As noted, the active state of GAOX contains a Tyrosine radical, coupled to the Cu^{2+} centre. The Tyr radical is not, however, EPR active under normal experimental conditions. EPR spectra previously recorded for this enzyme are therefore mainly contributed by the Cu^{2+} centre and its local environments.[2] In the present work, EPR spectra of the free GAOX samples were measured for the frozen solution state at the X-band (approx. 9 GHz) at 8 K. The spectrum is a typical tetragonal axial spectrum for Cu^{2+} and was simulated using a spin Hamiltonian model with $S =$

½ and hyperfine coupling to ^{65}Cu and ^{63}Cu nuclei (both I = 3/2). The parameters used in the fit were $g_{\|}$ = 2.26(1), $g_{\perp}$ = 2.07(1), $A_{\|}$ = 500(20) MHz and $A_{\perp}$ = 45(40) MHz. In comparison with literature values for GAOX[2, 59, 60], $g_{\|}$ was found to be slightly lower (2.26(1) compared to 2.27-2.30) whereas the other parameters are consistent with the reported values.

The GAOX-MPS samples were prepared as described above. EPR spectra at room temperature (RT) and at several lower temperatures down to 8 K were recorded. The spectrum of the immobilized GAOX in the evacuated solid state at 8 K is shown in Fig. 3 (left, blue curve; the zoom-in top right, blue curve). The EPR spectrum is very similar to that for unconfined GAOX but detailed analysis discloses at least two different Cu species. The major species was found to constitute up to (75(±10) %) by the simulation analysis with the parameters $g_{\|}$ = 2.33(1), $g_{\perp}$ = 2.06(1), $A_{\|}$ = 425(20) MHz and $A_{\perp}$ = 40(35) MHz. The minor species was found to be (25(±10) %) from the simulation with the parameters $g_{\|}$ = 2.39(2), $g_{\perp}$ = 2.06(1)), $A_{\|}$ = 375(20) MHz and $A_{\perp}$ = 40(35) MHz, but is less well determined possibly due to the presence of more than a single minor species. The spectrum of the immobilized GAOX in buffered suspension is also shown in Fig. 3 (left, green curve). The same two species were found but in a different ratio, i.e. ~65 % of the previous minor species with high $g_{\|}$ and $A_{\|}$ and only ~35 % of the previous major species with low $g_{\|}$ and $A_{\|}$. The key parameters obtained by the simulations are summarized in Table 2. Both species in the immobilized phases thus have significantly higher $g_{\|}$ but significantly lower $A_{\|}$ than the free protein in frozen solution. Traces of a radical signal at g = 2.00 are visible for all spectra

The spin Hamiltonian parameters of the GAOX at 8-10 K in both free and immobilized states correspond to Type 2 copper proteins and biomimetic copper complexes with a tetragonal coordination environment consisting of two nitrogen donors and two oxygen donors in a plane and one or two more remote axial donors. After immobilization the EPR parameters of GAOX are shifted significantly towards higher $g_{\|}$ and lower $A_{\|}$ which still describes the same donor set. Two species are visible in different ratios in both the evacuated immobilized solid and the suspension. The observed shift in parameters can either correspond to a higher net charge on the coordination site or a distortion away from planarity of the 2N2O coordination core[61, 62]. It is likely that the negative charges on the support silica could shift the total charge on the immobilized protein towards a more positive value compared to the free protein in solution. The effect is more pronounced in the suspended state where plenty of water molecules are present as a polar medium compared to the evacuated solid state.

The solid evacuated sample with immobilized GAOX gave a spectrum with clear evidence of both an anisotropic and an isotropic Cu species at RT, Fig.3 (bottom right). Simulations provided well determined parameters g_{iso} = 2.15(1), A_{iso} = 160(15) for the isotropic species and an estimate of $g_{\|}$ = 2.26, $g_{\perp}$ = 2.07, $A(\mathrm{Cu})_{\|}$ = 470 MHz and $A(\mathrm{Cu})_{\perp}$ = 45 MHz for the anisotropic species with features partially covered by the isotropic spectrum. The distribution between the two species was estimated from simulation to be 25-40 % of the isotropic and 75-60 % of the anisotropic species. The spin Hamiltonian parameters for GAOX are shifted as the temperature changes[63] but the isotropic species at RT still corresponds better to the major species than to the minor species at 10 K. The presence of an isotropic signal at room temperature indicates that a substantial percentage (25-40%) of the

EPR active copper centers are able to rotate or at least change their unique axis freely, whereas the rest shows restricted rotation on the EPR time scale (~10^{10} Hz).

Catalytic activity and kinetics. Immobilization of the enzyme in MPS via physical confinement or ionic binding is relatively weak. As a consequence, enzyme leaching could occur during activity measurements. To test possible enzyme leaching, the SBA-15-ROD-GAOX conjugate was stirred at 475 rpm at room temperature for 2-3 hours, i.e. experimental conditions similar to those used for the activity measurements. The results show that there is no detectable leaching. This is supported by the fact that the supernatants obtained from the leaching test experiments show no enzyme activity. In contrast, significant enzyme leaching was observed for GAOX physically confined in MCF without amination with larger pore size (23 nm) during the tests. The catalytic activity of the supernatants obtained from the leaching test experiments could account for up to 63 % of total activity before leaching, i.e. over 60% enzyme was released from the MPS pores. This observation suggests that a matching pore size is crucial to confine the enzyme located inside the pore by physical trapping. Due to its much larger pore sizes (23 nm) than enzyme dimension (around 8.5 nm, Fig. 1d), MCF can lead to unstable GAOX trapping. Other factors can, however, affect the stability. Once the enzyme is confined inside pores, its stability thus depends on both pore size and interactions (e.g., electrostatic attraction) between enzyme molecules and pore walls. Structural properties of MPS are thus certainly important too. Compared to SBA-15-ROD, MCF has a smaller surface area available for interacting enzyme because the surface curvature is lower than for SBA-15. The number of ionic bonds between the enzyme and silica pores would thus be significantly smaller, which also accounts for leaching.

To prevent the enzyme leaching from MCF, covalent attachment of the enzyme on MCF was used as an improved approach. To this end, MCF was first functionalized with amine groups, followed by covalent attachment of GOAX to MCF using cyanuric chloride. Similar leaching test experiments as for non-covalently immobilized enzyme were carried out and showed no detectable enzyme activity in the supernatants.

The catalytic activity of GAOX was estimated by measuring the dioxygen consumption. The decrease of dioxygen concentration in solution over the time course was recorded, with systematic comparison of three types of samples i.e. free GAOX, SBA-15-ROD-GAOX and MCF-GAOX (Figure S4, Supplementary Information). Note that the catalytic reaction of GAOX is a bi-substrate reaction. To determine key catalytic constants of free and immobilized enzyme, the initial reaction rates were recorded over a range of substrate (galactose) concentrations while the initial concentration of the other substrate, dioxygen, is kept constant. Figure 4 compares typical Michaelis-Menten plots for free and immobilized enzyme samples. The solid lines show the theoretical fittings based on the Michaelis-Menten equation (eq.(5)), i.e.

$$\upsilon = \frac{V_{\max}[\mathrm{S}_0]}{K_M + [\mathrm{S}_0]} \qquad (5)$$

where υ is the (initial) rate of enzyme catalyzed conversion and $[S_0]$ the initial substrate concentration. The maximum rate constant (V_{max}), apparent Michaelis constant (K_M) and turnover number (k_{cat}) summarized in Table 3 were obtained from this equation. k_{cat}/K_M is used as a measure of the overall catalytic efficiency [64]. The enzyme in SBA-15-ROD and MCF retains 70 % and 60% catalytic efficiency upon immobilization, respectively.

Evaluation of thermal stability. The thermal stability of GAOX physically confined in SBA-15-ROD (SBA-15-ROD-GAOX) and covalently attached to MCF (MCF-GAOX) was examined by heating the solution of MPS-GAOX for 30 min in the temperature range 50-70°C.[46] The solution was then left for cooling to room temperature, and the catalytic activity assayed at 25°C. The free enzyme was treated similarly for comparison. Figure 5 compares the catalytic activity of free and confined enzyme at different temperatures used in solutions heated. SBA-15-ROD-GAOX and covalent MCF-GAOX and shows that confined enzyme retains 85-88% activity, when temperatures were elevated up to 50-55°C, while free enzyme retains 75-80% activity. Detectable enhancement is thus observed up to 55-60 °C, but no further enhancement above 60 °C. Both free and immobilized enzymes lost over 90% activity after heating at 70 °C or above for 30 min. This observation accords with the transition temperature for stability of this enzyme. Intracellular GAOX has a stability transition temperature around 60 °C[65], but notably lower for the extracellular form (45-50 °C) because the former contains more carbohydrate components. GAOX used in the present study is in the extracellular form.

An overview of literature reports for enzymes immobilized on MPS shows that thermal resistance depends in subtle ways on the individual enzymes and types of MPS. Some enzymes are more thermally resistant than their free state in solution[66-68]. For example, HRP is much more thermally stable in its immobilized state in MPS[46]. More recently, Chen et al.[69] reported that thermostability of glucose oxidase entrapped in a functionalized FSM via non-covalent interaction (predominantly through electrostatic interactions) is enhanced significantly. In contrast, many other enzymes have not shown significant improvement in thermostability. For example, chloroperoxidase immobilized on MPS does not show any enhancement in thermal stability[70]. The behaviour of α-amylase[54] is more complex. No enhancement in thermal resistance is observed on immobilization on SBA-15. However, thermal stability is significantly improved when immobilized on folded-sheet mesoporous silica (FSM). This is most likely due to different hydrophilicity of SBA-15 and FSM pores, which results in different interactions between this enzyme and MPS pores. Stability of proteins is a delicate balance of different interactions with non-covalent interactions dominating. Among various non-covalent interactions, electrostatic stabilization appears to play a key role in enhanced thermostability for many proteins.[71]

The size-matching of MPS pores and enzymes is considered one of the major means of enhancing thermal stability of immobilized enzymes[72]. However, SBA-15-ROD-GAOX did not show significant enhancement in resistance to heat. Covalent attachment is another means to enhance thermal stability of immobilized enzymes by reducing conformational flexibility and thermal vibrations[73]. Covalently immobilized GAOX on MCF (MCF-GAOX) did not, however, show significantly improved resistance to heat either. For the immobilized enzyme to be structurally rigid, selection of the support, reactive group and immobilization conditions are critical[16-18]. The

enzyme and support should have a great congruence so that strong attachment is favoured[74]. In this respect, however, neither the result obtained in the present work nor the report that chloroperoxidase (CPO) covalently immobilized on SBA-16 (having cage-like structure similar to that of MCF) using succinic anhydride as a coupling reagent showed enhanced heat resistance[75]. This indicates that certain enzymes and MPS having cage-like structure have low congruence. It is reported that thermal stability of covalently immobilized enzyme depends on the coupling reagent (reactive group)[76]. For example, glucose oxidase (GOD) immobilized by cyanuric chloride on the NH_2-glass loses approximately half its activity after treatment at 65°C for 30 min, while GOD immobilized by isophthalaldehyde and 1,3-diacetylbenzene on NH_2-glass loses as much as 100% (note that native free GOD lost more than 70% of its initial activity under the same condition.). In the present study, GAOX was covalently immobilized on MCF by cyanuric chloride. Cyanuric chloride was selected based on previous reports on successful use of this coupling agent (e.g. Ref. 12). This organic spacer and GAOX may not be the best combination to enhance thermal stability. One of the main reasons is most likely that the linker agent used (i.e. cyanuric chloride) is unable to create multipoint attachment of GAOX to inside the pores. Thus, once enzyme is partially denatured upon heating, the interaction with the silica surface could thus cause irreversible changes. The native structure of the enzyme cannot therefore be fully recovered even if the confined protein is cooled down to room temperature[73].

4. Conclusions

GAOX was confined in two types of mesoporous silicas, one with hexagonally ordered pore structure (SBA-15-ROD), the other one with a mesocellular foam like structure with larger but randomly distributed pores (23 nm) interconnected by narrower windows (8.8 nm) (MCF). Size matching of the pore and enzyme prevented leaching of GAOX from SBA-15-ROD, while covalent attachment is needed to prevent the leaching of GAOX from MCF. EPR analysis revealed that electronic structure and coordination sphere of immobilized GAOX are well preserved. Immobilized enzyme retains catalytic activity, but thermostability of this enzyme is not significantly enhanced by nanoscale confinement above 60 ^{o}C.

As summarized in a recent review by Magner[42], mesoporous silicates as a support for enzyme immobilization have shown the advantages and drawbacks. The present study on GAOX has supported the view that the effects of immobilization are unique for each enzyme, although many immobilization methods have been developed. As noted, GAOX is a complex enzyme in both structure and catalytic mechanisms. The present work represents the first attempt to study this enzyme confined in MPS materials using both advanced structural probing and catalytic characterization. However, from an application point of view the performance of immobilized GAOX including catalytic activity and thermal stability needs to be improved. This could be achieved by optimizing design and synthesis of MPS materials structurally better compatible with the enzyme as well as enzyme immobilization procedure including selection of cross-linker agents.

Acknowledgements

This work was supported by the Lundbeck Foundation (Grant No. R49-A5331, to Q.C.) and the Danish Research Council for Technology and Production Sciences (FTP, Project No. 274-07-0272, to J.U. and Q.C.). S.M. acknowledges the financial support from the Danish Council for Independent Research, Technology and Production Sciences. The authors thank the staff at the Center of Electron Nanoscopy at DTU for their assistance in the SEM and TEM measurements, Helge Kildahl Rasmussen at DTU Physics for help in the XRD experiments, and Rasmus Fehrmann and his group at DTU Chemistry for assistance in the dinitrogen adsorption/desorption measurements.

Notes and References

[a] *Department of Chemistry,Technical University of Denmark, DK-2800 Kongens Lyngby, Denmark.*
E-mail: cq@kemi.dtu.dk; Tel: +45-4525-2032; Fax: +45-4588-3136

Electronic Supplementary Information (ESI) available: Figure S1 illustrates schematically the catalytic mechanisms of galactose oxidase. Figure S2 shows a schematic diagram of the dioxygen monitoring system. Figures S3 to S5 and Table S1 provide the data for the synthesis and characterization of mesoporous silicas. Figure S6 shows FT-IR spectra of SBA-15-TMB before and after functionalization with amine and methyl groups. Figure S7 shows examples of kinetic response curves of enzyme to substrate galactose in free and immobilized states. See DOI: 10.1039/b000000x/

1 J. W. Whittaker, *Chem. Rev.,* 2003, **103**, 2347-2363.
2 M. M. Whittaker and J. W. Whittaker, *J. Biol. Chem.,* 1988, **263**, 6074-6080.
3 N. Ito, S. E. V. Phillips, C. Stevens, Z. B. Ogel, M. J. McPherson, J. N. Keen, K. D. S. Yadav, and P. F. Knowles, *Nature*, 1991, **265**, 9610-9613.
4 S. Itoh, S. Takayama, R. Arakawa, A. Furuta, M. Komatsu, A. Ishida, S. Takamuku and S. Fukuzumi, *Inorg. Chem.,* 1997, **36**, 1407-1416.
5 D. Rokhsana, D. M. Dooley, and R. K. Szilagy, *J. Am. Chem. Soc.,* 2006, **128**, 15550-15551.
6 P. Tressel, and D. Kosman, *J. Aanal. Biochem.,* 1980, **105**, 150-153.
7 J. A. D. Cooper, W. Smith, M. Bacila, and H. Medina, *J. Biol. Chem.,* 1959, **234**, 445-453.
8 K. J. Humphreys, L. M. Mirica, Yi. Wang and J. P. Klinman, *J. Am. Chem. Soc*., 2009, **131**, 4657–4663.
9 E. Çevik, M. Şenel and M. F. Abasıyanık, *Curr. Appl. Phys.,* 2010, **10**, 1313-1316.
10 S. K. Sharma, C. S. Pundir, N. Sehgal and A. Kumar, *Sens. Actuators B* 2006, **119**, 15–19.
11 Z. Bílková, M. Slováková, A. Lyčka, D. Horák, J. Lenfeld, J. Turková and J. Churáček, *J. Chromatogr. B* 2002, **770**, 25–34.
12 L. Kondakova, V. Yanishpolskii, V. Tertykh and T. Buglova, *Anal. Sci.* 2007, **23**, 97-101.

13 J. M. Nelson and E. G. Griffin, *J. Am. Chem. Soc.,* 1916, **38**, 1109-1115.
14 O. Barbosa, C. Ortiz, A. Berenguer-Murcia, R. Torres, R. C. Rodrigues and R. Fernández-Lafuente, *RSC Adv.*, 2014, **4**, 1583–1600.
15 R. C. Rodrigues, C. Ortiz, A. Berenguer-Murcia, R. Torres and R. Fernández-Lafuente, *Chem. Soc. Rev.*, 2013, **42**, 6290 – 6307.
16 K. Hernandez, A. Berenguer-Murcia, R. C. Rodrigues and R. Fernández-Lafuente, *Curr. Org. Chem.,* 2012, **16**, 2652 – 2672.
17 O. Barbosa, R. Torres, C. Ortiz, A. Berenguer-Murcia, R. C. Rodrigues and Fernandez-Lafuente, R., *Biomacromolecules*, 2013, **14**, 2433-2462.
18 C. Garcia-Galan, A. Berenguer-Murcia, R. Fernandez-Lafuente and R. C. Rodrigues, *Advanced Synthesis and Catalysis*, 2011, **353**, 2885-2904.
19 C. Mateo, J. M. Palomo, G. Fernandez-Lorente, J. M. Guisan, R. Fernandez-Lafuente, *Enzyme and Microbial Technology*, 2007, **40**, 1451-1463.
20 M. L. Verma, C. J. Barrow, M. Puri, *Appl. Microb. Biotech.*, 2013, **97**, 23-39.
21 E. T. Hwang, M. B. Gu, *Eng. in Life Sci.*, 2013, **13**, 49-61.
22 C. T. Kresge, M. E. Leonowicz, W. J. Roth, J. C. Vartuli and J. S. Beck, *Nature*, 1992, **359**, 710-712.
23 D. Y. Zhao, J. Feng, Q. Huo, N. Melosh, H. G. Fredrickson, F. B. Chmelka and D. G. Stucky, *Science*, 1998, **279**, 548-552.
24 M. E. Davis, *Nature*, 2002, **417**, 813-821.
25 F. Hoffmann, M. Cornelius, J. Morell and M. Fröba, *Angew. Chem. Int. Ed.*, 2006, **45**, 3216-3251.
26 Y. Wan and D. Y. Zhao, *Chem. Rev.*, 2007, **107**, 2821-2860.
27 K. K. Coti, M. E. Belowwich, M. Liong, M. W. Ambrogio, Y. A. Lau, H. A. Khatib, J. I. Zink, N. M. Khashab and J. F. Stoddart, *Nanoscale*, 2009, **1**, 16-39.
28 K. E. Shopsowitz, H. Qi, W. Y. Hamad and M. J. MacLachlan, *Nature*, 2010, **468**, 422-425.
29 Y. Wang, A. D. Price and F. Caruso, *J. Mater. Chem.*, 2009, **19**, 6453 – 6464.
30 J. F. Díaz, K. J. Jr. Balkus, *J. Mol. Catal. B: Enzym.*, 1996, **2**, 115-126.
31 M. Hartman, *Chem. Mater.*, 2005, **17**, 4577 - 4593.
32 S. Hudson, J. Cooney and E. Magner, *Angew. Chem. Int. Ed.* 2008, **47**, 8582-8594.
33 C. Ispas, I. Sokolov and S. Andreescu, *Anal. Bioanal. Chem.* 2009, **393**, 543-554.
34 D. N. Tran, K. J. Jr. Balkus, *ACS Catalysis*, 2011, **1**, 956-968.
35 F. Tang, L. Li and D. Chen, *Adv. Mater.*, 2012, **24**, 1504-1534.
36 B. Lebeau, A. Galarneau and M. Linden, *Chem. Soc. Rev.*, 2013, **42**, 3661-3662.
37 C. T. Kresge and W. J. Roth, *Chem. Soc. Rev.*, 2013, **42**, 3663-3670.
38 S.-H. Wu, C. Y. Mou and H. P. Lin, *Chem. Soc. Rev.*, 2013, **42**, 3862-3875.

39 P. Van der Voort, D. Esquivel, E. D. Canck, F. Goethals, I.Van Driesscheb and F. J. Romero-Salgueroc, *Chem. Soc. Rev.*, 2013, **42**, 3913-3955.

40 Y. Deng, J. Wei, Z. Sun and D. Y. Zhao, *Chem. Soc. Rev.*, 2013, **42**, 4054 – 4070.

41 U. Hanefeld, L. Cao and E. Magner, *Chem. Soc. Rev.*, 2013, **42**, 6211 – 6212.

42 E. Magner, *Chem. Soc. Rev.*, 2013, **42**, 6213 – 6222.

43 M. C. R. Franssen, P. Steunenberg, E. L. Scott, H. Zuilhof and J. P. M. Sanders, *Chem. Soc. Rev.*, 2013, **42**, 6491 – 6533.

44 Z. Zhou and M. Hartmann, *Chem. Soc. Rev.*, 2013, **42**, 3894 – 3912.

45 M. Hartmann and X. Kostrov, *Chem. Soc. Rev.*, 2013, **42**, 6277 – 6289.

46 H. Ikemoto, Q. Chi and J. Ulstrup, *J. Phys. Chem.* C, 2010, **114**, 16174–16180.

47 O. V. Lomako, I. I. Menyailova, L. A. Nakhapetia, L. I. Kozlovska and N. A. Rodioxova, *Acta Biotechnol.* 1982, **2**, 179-185.

48 C. Lei, Y. Shin, J.K. Magnuson, G.E. Fryxell, L.L. Lasure, D.C. Elliott, J. Liu, and E.J. Ackerman. *Nanotechnology*, 2006, **17**, 5531-5538.

49 F. Neese, W. G. Zumft, W. E. Antholine and P. M. H. Kroneck, *J. Am. Chem. Soc.*, 1996, **118**, 8692–8699.

50 C. D. Borman, C. G. Saysell and A. G. Sykes, *J. Biol. Inorg. Chem.*, 1997, **2**, 480-487.

51 M. S. Rogers, E. M. Tyler, N. Akyumani, C. R. Kurtis, R. K. Spooner, S. E. Deacon, S. Tamber, S. J. Firbank, K. Mahmoud, P. F. Knowles, S. E. V. Phillips, M. J. McPherson and D. M. Dooley, *Biochemistry*, 2007, **46**, 4606-4618.

52 S. J. Firbank, M. S. Rogers, C. M. Wilmot, M. A. Halcrow, P. F. Knowles, M. J. McPherson and S. E. V. Phillips, *Proc. Nat. Acad. Sci. USA,* **2001**, *98*, 12932-12937.

53 H. Takahashi, B. Li, T. Sasaki, C. Miyazaki, T. Kajino and S. Inagaki, *Micropor. Mesopor. Mater.,* 2001, **44**, 755–762.

54 K. Hisamatsu, T. Shiomi, S. Matsuura, T. Y. Nara, T. Tsunoda, F. Mizukami and K. Sakaguchi, *J. Porous Mater.*, 2012, **19**, 95–102.

55 E. Webera, D. Sirima, T. Schreiberb, B. Thomasb, J. Pleiss, M. Hungerb, R. Glaserc and V. B. Urlacher, *J. Mol. Catal. B: Enzym.*, 2010, **64**, 29–37.

56 A. Galarneau, M. Nader, F. Guenneau, F. D. Renzo and A. Gedeon, *J. Phys. Chem. C*, 2007, **111**, 8268–8277.

57 H. Ikemoto, S. Tubasum, T. Pullerits, J. Ulstrup and Q. Chi, *J. Phys. Chem.* C, 2013, **117**, 2868 – 2878.

58 Y.-W. Huang, Y.-C. Lai, C.-J. Tsai and Y.-W. Chiang, *Proc. Natl. Acad. Sci. USA*, 2011, **108**, 14145 – 14150.

59 L. Cleveland, R. E. Coffman, P. Coon, L. Davis, *Biochemistry*, 1975, **14**, 1108-1115.

60 D. J. Kosman, R. D. Bereman, M. J. Ettinger and R. S. Giordano, *Biochem. Biophys. Res. Commun.*, 1973, **54**, 856-861.

61 U. Sakaguchi and A. W. Addison, *J. Chem. Soc, Dalton Trans.*, 1979, **4**, 600-608.
62 J. Peisach and W. E. Blumberg, *Arch. Biochem. Biophys.*, 1974, **165**, 691-708.
63 M. M. Whittaker and J. W. Whittaker, *Biophys. J.*, 1993, **64**, 762-772.
64 D. Voet and J. G. Voet, in *Biochemisty*, John Wiley & Sons, Inc., 2nd Ed., 1995, pp. 351-354.
65 M. H. Mendonca and G. T. Zancan, *Arch. Biochem. Biophys.* 1988, **266**, 427-434.
66 Y. Urabe, T. Shiomi, T. Itoh, A. Kawai, T. Tsunoda, F. Mizukami and K. Sakaguchi, *Chem Bio Chem*, 2007, **8**, 668- 674.
67 C.H. Lee, J. Lang, C.W. Yen, P.C. Shih, T.S. Lin and C.Y. Mou, *J. Phys. Chem.* B, 2005, **109**, 12277-12286.
68 E. Terrés, M. Montiel, S. Le Borgne and E. Torres, *Biotechnol Lett*. 2008, **30**, 173-9.
69 B. Chen, W. Qi, X. Li, C. Lei and J. Liu, *Small*, 2013, **9**, 2228-2232.
70 Y-J. Han, J. T. Watson, G. D. Stucky and A. Butler, *J. Mol. Catal. B: Enzym.*, 2002, **17**, 1–8.
71 A. Karshikoff and R. Ladenstain, in *Methods in Protein Structure and Stability Analysis: Conformational Stability, Size, Shape and Surface of Protein Molecules*, ed. V. N. Uversky and E. A. Permyakov, Nova Science Pub Inc, 2007, pp. 74.
72 A. H. Lee, T. S. Lin and C. Y. Mou, *Nano Today*, 2009, **4**, 165-179.
73 U. Hanefeld, L. Gardossib and E. Magner, *Chem. Soc. Rev.*, 2009, **38**, 453–468.
74 J. Pedroche, M. del Mar Yust, C. Mateo, R. Fernandez-Lafuente, J. Giron-Calle, M. Alaiz, J. Vioque, J. M. Guisan, F. Millan, *Enzyme Microb. Technol.*, 2007, **40**, 1160–1166.
75 J. Aburto, M. Ayala, I. Bustos-Jaimes, C. Montiel, E. Terrés, J. M. Domínguez and E. Torres, *Microporous Mesoporous Mater.*, 2005, **83**, 193-200.
76 J. C. Tiller, R. Rieseler, P. Berlin and D. Klemm, *Biomacromolecules*, 2002, **3**, 1021-1029.

TABLE 1. Physical characteristics of mesoporous silicas and enzyme loading.

Mesoporous silicas	S_{BET} ($m^2\ g^{-1}$)	V_{tot} (cm^3/g)	D_p (nm)	D_w (nm)	*Enzyme loading amount* (mg per g silica)
SBA-15-ROD	840	1.26	9.5	NA	62
MCF	810	2.12	23.1	8.8	58

S_{BET}: Total surface area; V_{tot}: Total pore volume; D_p: Pore diameter, determined by the BJH method from the adsorption Branch; D_w: Window diameter, determined by the BJH method from the desorption branch of the nitrogen adsorption isotherm.

TABLE 2. Comparison of spin Hamiltonian parameters in the simulation of GAOX from the spectra obtained at 8-10 K[a].

	$g_{\|}$	$g_{\perp}$	$A_{\|}$ / MHz	$A_{\perp}$ / MHz	Solution	Immobilized GAOX, evac. solid	Immobilized GAOX, suspension
Species 1	2.26(1)	2.07(1)	500(20)	45(40)	~100 %	-	-
Species 2	2.33(1)	2.06(1)	425(20)	40(35)	-	~75 %	~35%
Species 3	2.39(2)	2.06(1)	375(20)	40(35)	-	~25 %	~65 %
Reported values*	2.27-2.30	2.06-2.07	500-525	15-80	~100 %	-	-

[a] Three species are observed in different ratios depending on the preparation method. $A_{\perp}$ is not resolved and therefore has a relatively high uncertainty. * The values reported in Refs. 2, 54 and 55, with the EPR spectra recorded under the temperatures between 30 and 110 K.

TABLE 3. Comparison of the catalytic characteristics of GAOX in free and confined states.

Enzyme states	V_{max} (nmol min^{-1})	K_M (mM)	k_{cat} (s^{-1})	k_{cat}/K_M ($M^{-1}\ s^{-1}$)
Free state	86 ± 10	50	7.9	160
Confined in SBA-15-rod [a]	44 ± 7	59	6.7	110
Confined in MCF[b]	42 ± 8	66	6.2	94

[a] Enzyme is physically trapped in silicas. [b] Enzyme is covalently attached to MPS.

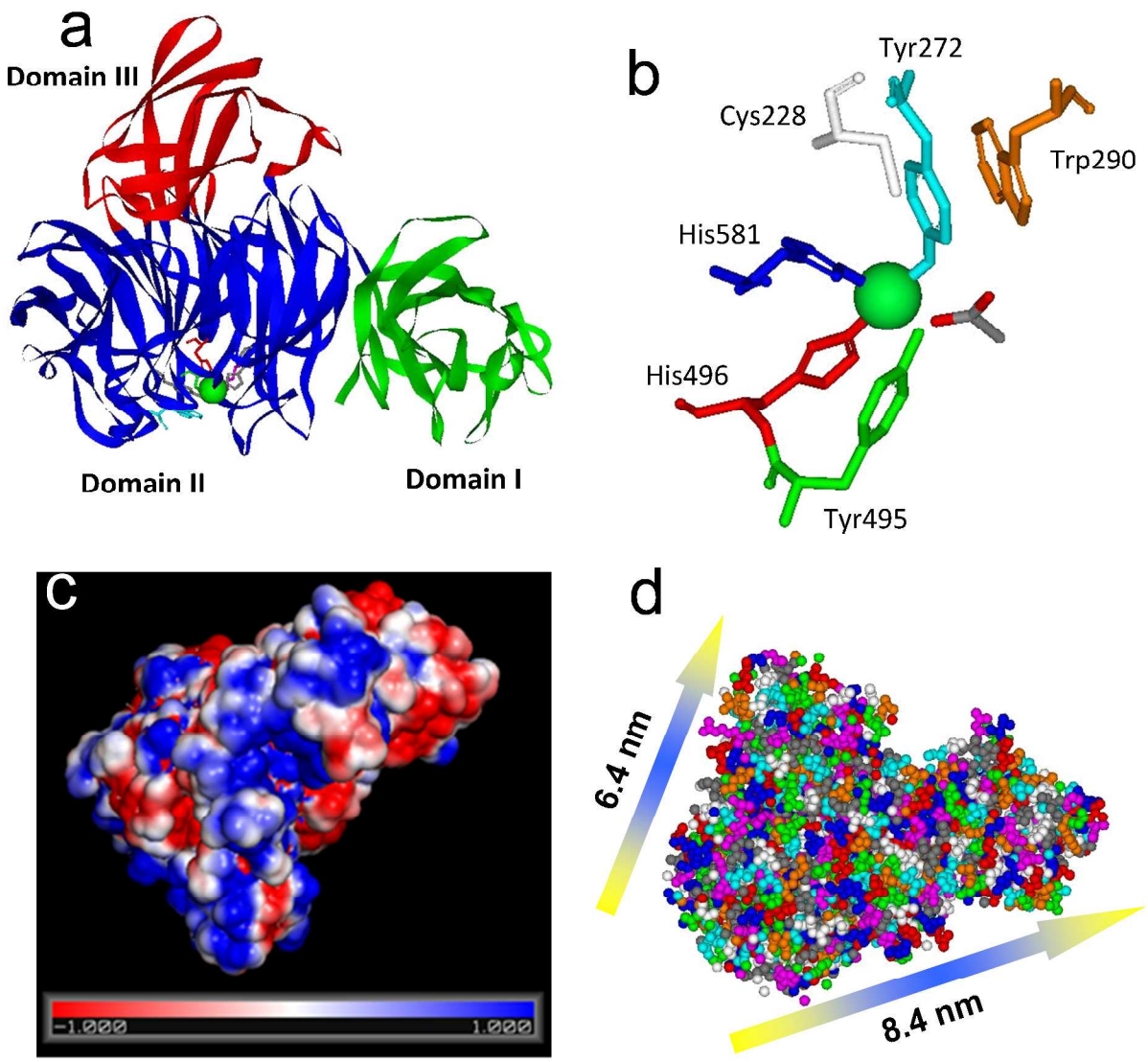

Figure 1. Structures of galactose oxidase from *Dactylium dendroides*. (a) Three-dimensional structural representation of the enzyme with the three domains noted. (b) The detailed structure of the catalytic active site. (c) The distribution of electrostatic potential of the enzyme at pH 7.0. Positive surface charge is shown in blue and negative surface charge in red. The surface charge distribution is obtained through electrostatic calculations carried out using Adaptive Poisson-Boltzmann Solver (APBS) after conversion of the PDB file to the PQR file through PDB2PQR Server and visualized with Pymol. (d) Three-dimensional atomic ball model of the enzyme with the key lateral dimensions noted. (PDB file: 1gog).

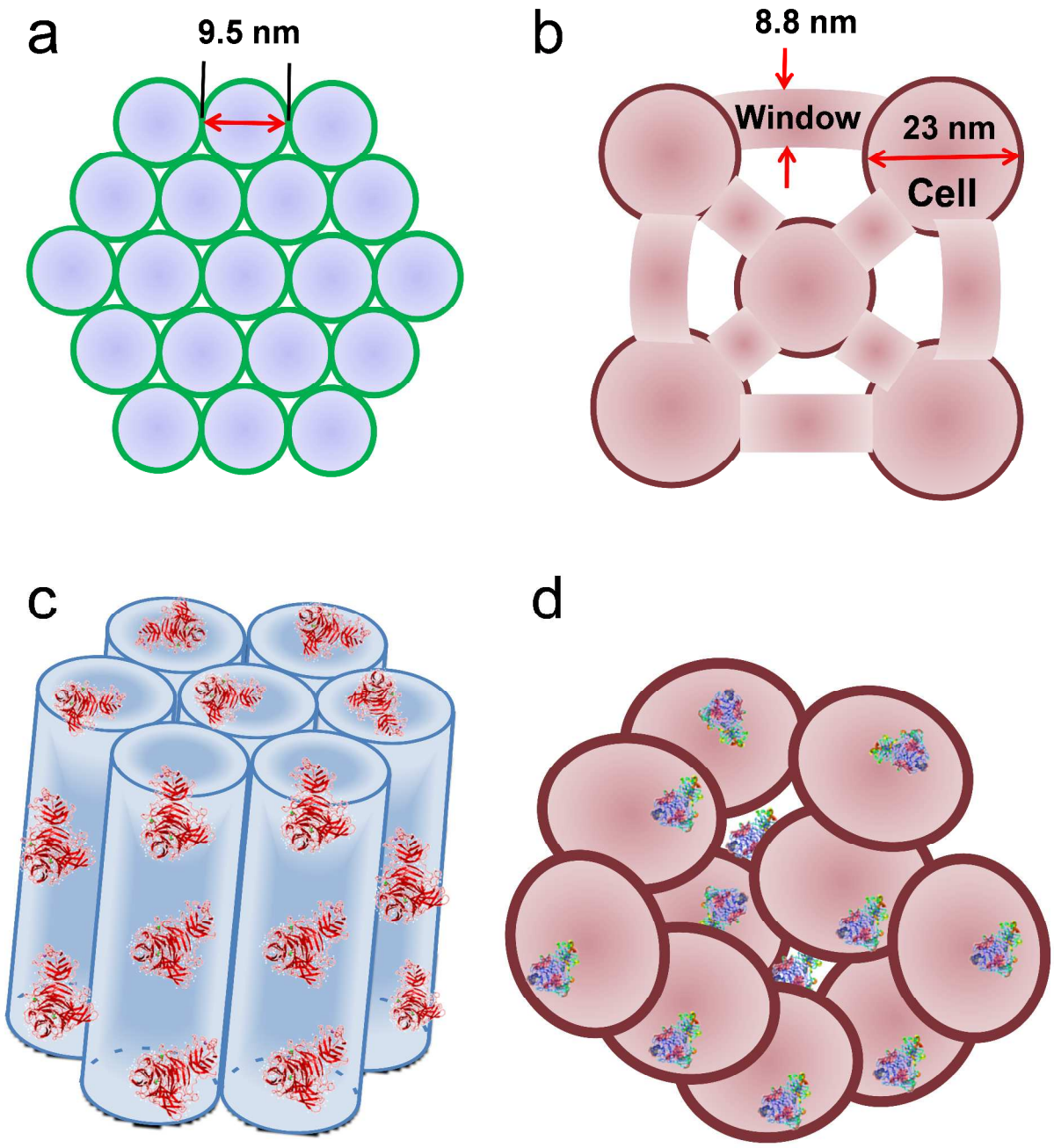

Figure 2. Schematic illustration of two-dimensional top-view structures (a, b) and of three-dimensional view (c, d) of enzyme molecules confined in the pores of MPS. (a, c) SBA-15-ROD with cylinder pores (9.5 nm) in ordered arrays. (b, d) MCF with larger pores (23 nm) interconnected by 8.8 nm windows. Possible locations of enzyme are proposed. Not drawn to scale.

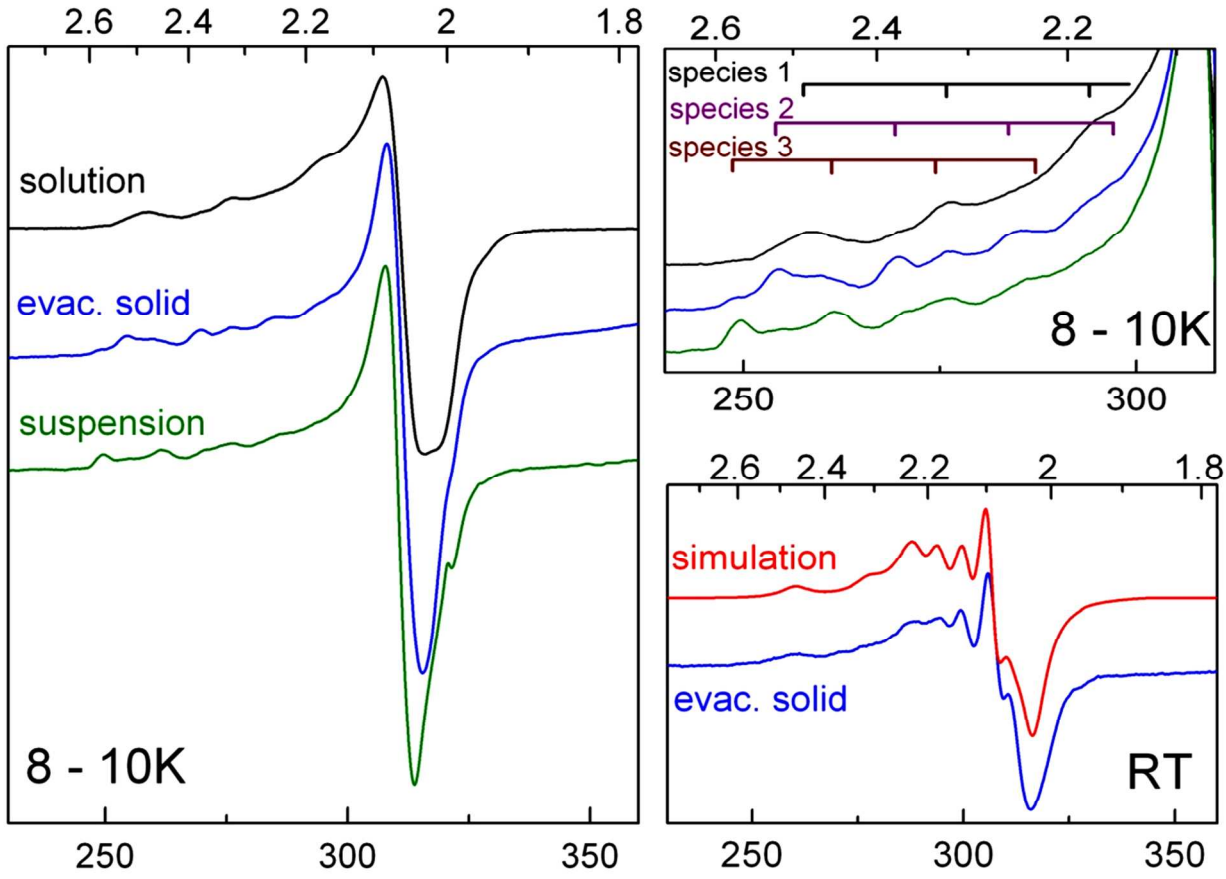

Figure 3. Comparison of EPR spectra for free enzyme and the enzyme-silica conjugates. Left: GAOX enzyme in frozen buffered solution, 8 K, evacuated solid, 10 K and solid in buffered suspension, 10 K. Top right: Zoom-in on the hyperfine splittings of the parallel part of the spectra. Bottom right: Evacuated solid measured at room temperature and spin Hamiltonian based simulation with the assumption of 30 % of an isotropic copper species and 70 % of an anisotropic copper species. The simulation parameters used are detailed in the text.

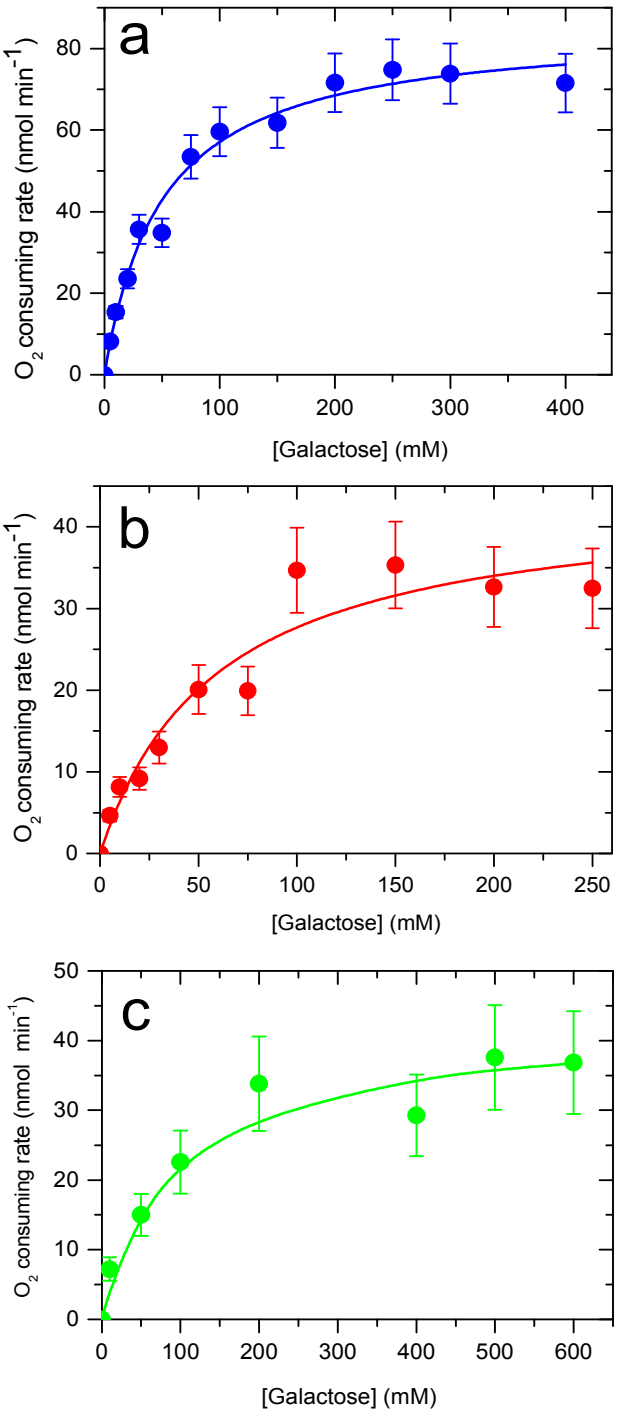

Figure 4. Plots of initial catalytic velocity vs galactose substrate concentration for (a) free, (b) SBA-15-ROD-GAOX, and (c) MCF-GAOX. Free or immobilized enzyme was mixed with phosphate buffer solutions (100 mM, pH 7.0) containing galactose in different concentrations (5 - 600 mM) and $K_3[Fe(CN)_6]$ (1 mM). Fittings (solid lines) were obtained using the Michaelis-Menten rate constant form. The amounts of free and immobilized GAOX used were estimated as 0.18 nmol and 0.11 nmol, respectively.

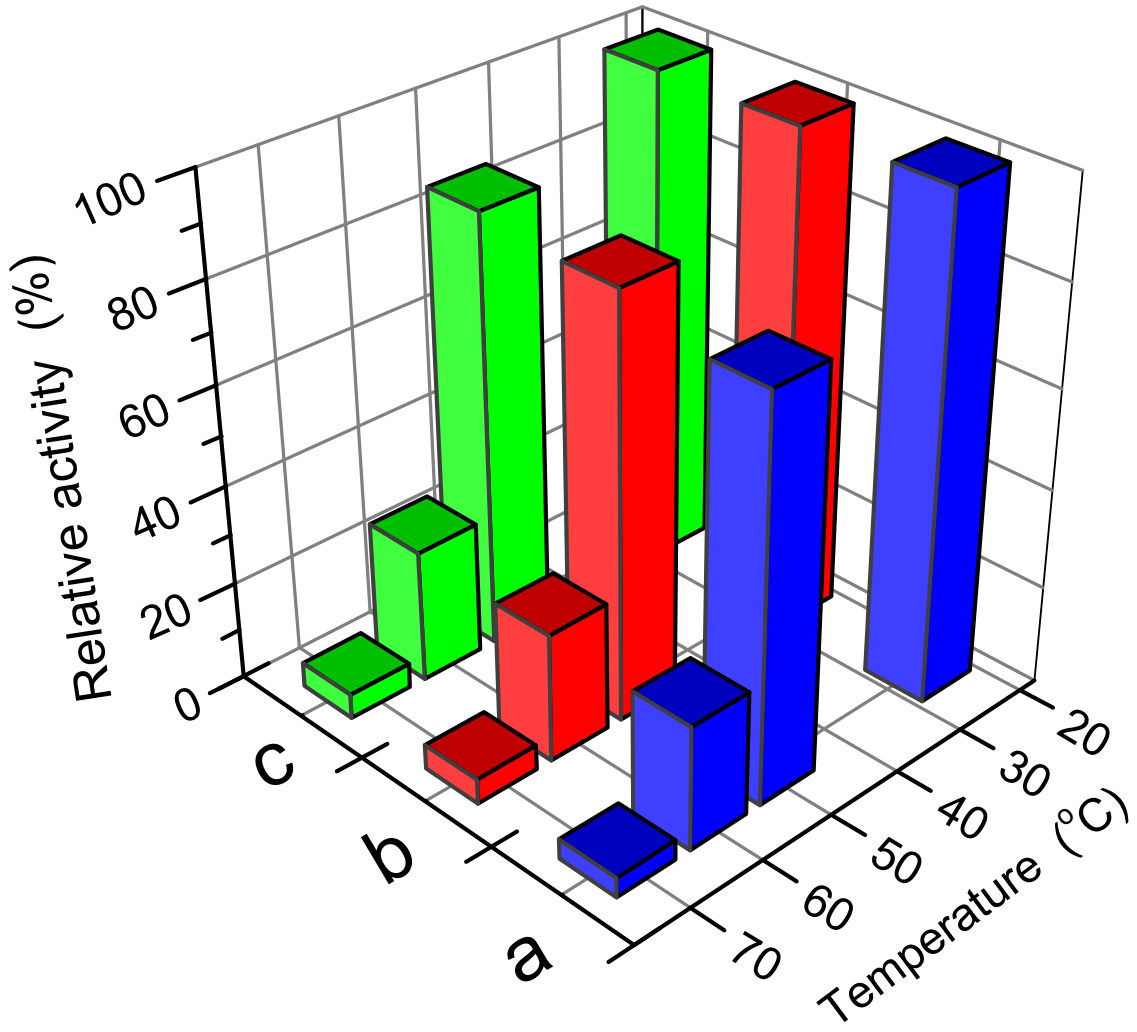

Figure 5. Comparison of the catalytic activity between free and immobilized GAOX after heat treatment at 50-70 °C: (a) free GAOX (blue), (b) GAOX-SBA-ROD (red) and (c) GAOX-MCF (green). The catalytic activity at 25°C before the heating treatment is defined as 100% activity.

Table of Contents

Probing Structural and Catalytic Characteristics of Galactose Oxidase Confined in Nanoscale Chemical Environments

by Hideki Ikemoto, Susanne L. Mossin, Jens Ulstrup, and Qijin Chi

Graphic:

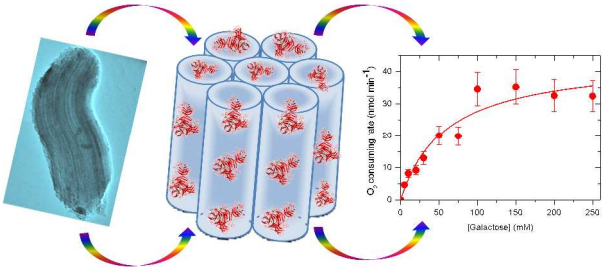

Size: 8 cm x 3.5 cm

Synopsis: *Structural and catalytic features of a complex enzyme galactose oxidase confined in nanoscale chemical environments were illuminated to show the catalytic efficiency of the enzyme depending on both the degree of space confinement and immobilization method.*

.

KEYWORDS: ***galactose oxidase, mesoporous silica, nanoscale confinement, enzyme biocatalysis, electron spin resonance.***